PeriodicPendulums

Adam Kanoun, Daniel Cowley, Victor Ivachtchenko
MAT332H5

December 2024

Contents

1 Introduction

Methods and algorithms are widely discussed in classical mechanics texts, particularly in the study of dynamical systems concerning their analysis, characterization, and simulation. Numerical experiments on Hamiltonian and non-Hamiltonian systems can be carried out with the application of symplectic, Dirac, and Borel-Laplace integrators, depending on the system of interest [Razafindralandy et al. 2019]. Furthermore, pre-existing and commonly used methods still have the potential of yielding new insights on dynamical systems [Calvão and Penna 2015].

Our study of pendulum systems utilizes various methods of symplectic integration, with the key interest of conserving the total energy of the system while it is in motion. Moreover, we are interested in analyzing the chaotic behaviour of these pendulum systems and its interaction with each of our selected integrators. To do so, we apply Lagrangian and Hamiltonian mechanics to derive differential equations describing the pendulum systems' motion. We will discuss our chosen methods of integration, including Euler's explicit and semi-implicit forms, Leapfrog, and Runge-Kutta. Our analysis was centred on our tailored simulations of pendulum systems using pygame and matplot; an interactive simulator which allows for the selection of initial conditions, as well as the collection and display of information pertinent to our study (e.g. kinetic energy, potential energy, time, etc.). Finally, we discuss the efficacy of each symplectic integrator based on our findings.

2 Hamiltonian Systems and Symplecticity

2.1 What Are Hamiltonian Systems?

A Hamiltonian system is a $2n$-dimensional dynamical system that appears when studying systems governed by the principle of conservation of energy. The Hamiltonian framework is important in understanding the geometry and long-term behavior of dynamical systems.

Hamiltonian Function and Equations of Motion

The Hamiltonian function $H(q, p, t)$ represents the total energy of the system as a function of generalized coordinates q, generalized momenta p, and time t. For many mechanical systems, $H(q, p, t)$ takes the form:

$$H(q, p, t) = T(p) + V(q),$$

where $T(p)$ and $V(q)$ represent the kinetic and potential energy, respectively.[1]

Furthermore, the evolution of the system is determined by Hamilton's equations (Meyer and Offin 2017, p. 5):

$$\dot{q}_i = \frac{\partial H}{\partial p_i}, \quad \dot{p}_i = -\frac{\partial H}{\partial q_i}.$$

Here, $\dot{q}$ and $\dot{p}$ describe the flow of the system in phase space. It is important to note that Hamiltonian systems are *non-dissipative*. This means that, by Liouville's theorem, the phase space area is preserved under the flow (Hairer, Wanner, and Lubich 2006, p. 227).

Time Independence and First Integrals

If the Hamiltonian function $H(q, p)$ does not explicitly depend on time t, the system is said to be autonomous (Q. Wang 2024, p. 7). In such cases, $H(q, p)$ itself is a conserved quantity,

[1] *Note*: Not all Hamiltonian functions can be decomposed into kinetic and potential energy parts. Indeed, there exists Hamiltonian systems where the Hamiltonian structure is well-defined, but the Hamiltonian function does not correspond to a mechanical system in a traditional sense (Q. Wang 2024, p. 79).

known as a *first integral*. This conservation follows from:

$$0 = \frac{\partial H}{\partial p}(-\frac{\partial H}{\partial q})^T + \frac{\partial H}{\partial q}(\frac{\partial H}{\partial p})^T$$

(Meyer and Offin 2017, p. 98)

2.2 Importance of Symplectic Integrators

Symplectic Structure

Recall from earlier, Hamiltonian systems are naturally defined on a $2n$-dimensional phase space with coordinates (q, p), where $q = (q_1, q_2, \ldots, q_n)$ and $p = (p_1, p_2, \ldots, p_n)$. The phase space is graced with a special geometric structure known as a *symplectic structure*. This structure helps ensure that the relationships between q and p are preserved during the system's evolution, thus maintaining the Hamiltonian nature.

The symplectic structure is described mathematically by a *symplectic 2-form*, denoted as:

$$\omega = \sum_{i=1}^{n} dp_i \wedge dq_i.$$

dp_i and dq_i are infinitesimal changes in momentum and position, respectively. On the other hand, $\wedge$ is the wedge product, which is a mathematical operation used to construct higher-dimensional objects from simpler ones. In this case, we can imagine it creating an"area element" in the phase space for each (q_i, p_i). Furthermore, the symplectic 2-form ω represents the geometry of the phase space and the relationships between q and p. Importantly, this structure is invariant under the flow of the Hamiltonian system. This is important, as it means that as the system evolves over time, the geometric relationships between q and p are preserved. Formally, if Φ^t represents the flow map of the system after time t, then:

$$(\Phi^t)^*\omega = \omega,$$

where $(\Phi^t)^*$ denotes a pullback of the symplectic form under the flow. (Meyer and Offin 2017; Hairer, Wanner, and Lubich 2006)

Symplectic Matrices and Hamiltonian Flows

An important property of Hamiltonian flows is that their Jacobian matrices $D\Phi^t$, satisfy the *symplectic condition*. In canonical coordinates, the symplectic structure is represented by a matrix J:

$$J = \begin{bmatrix} 0 & I_n \\ -I_n & 0 \end{bmatrix},$$

where I_n is an $n \times n$ identity matrix. Thus, a matrix M is symplectic if it satisfies:

$$M^T J M = J,$$

This ensures that the matrix preserves the symplectic structure, just as the flow map preserves ω. For the flow map Φ^t, its Jacobian $D\Phi^t$ satisfies this condition, guaranteeing the system's symplectic structure is preserved.

Symplectic Numerical Integrators

To do numerical simulations of Hamiltonian systems, requires a maintenance of the symplectic structure. This is crucial to accurately replicate the system's dynamics. Standard numerical methods like Explicit Euler can lead to phenomena such as artificial energy drift.

This is where symplectic integrators come into play. They are designed to secure the symplectic condition of the numerical flow $\tilde{\Phi}^t$:

$$(\tilde{\Phi}^t)^* \omega = \omega,$$

or equivalently, that the Jacobian of the numerical map is symplectic:

$$(D\tilde{\Phi}^t)^T J (D\tilde{\Phi}^t) = J.$$

2.3 Orders of Accuracy in Numerical Integration

The order of accuracy of a numerical integration method measures how closely the method approximates the true solution of a differential equation as the step size h approaches to zero. In general, higher-order methods produce smaller errors for a given step size, which allows for a greater precision and/or larger step sizes without sacrificing accuracy.

However, while higher-order methods do provide better accuracy, they often come at the cost of increased computational complexity, so a balance between precision and efficiency must be considered in practice.

2.4 Chosen Integration Methods

2.4.1 Explicit Euler

The explicit Euler integration method, developed by Euler in 1768, is the simplest numerical technique discussed. Its framework is expressed as

$$x_{n+1} = x_n + \Delta t \cdot f(x_n)$$

where a constant step size Δt is used to iteratively approximate the solution, starting from the initial condition $x(0) = x_0$. Such a formula represents a mapping (Hairer, Wanner & Lubich, 2006),

$$\Phi_t : x_n \mapsto x_{n+1}$$

Despite its ease of implementation, the explicit Euler method is susceptible to major drawbacks that will be discussed later.

2.4.2 Semi-implicit Euler

Similar to the explicit Euler method, the semi-implicit Euler integration, also known as the symplectic Euler, is used for partitioned systems where the update for the position depends on the velocity at the next time step

$$\dot{x} = a(u, v)$$
$$\dot{v} = b(u, v)$$

Giving us one possible formulation of the symplectic Euler method:

$$v_{n+1} = v_n + \Delta t \cdot a(x_n)$$
$$x_{n+1} = x_n + \Delta t \cdot v_{n+1}$$

Here, $a(x_n)$ represents the acceleration determined by the current position. Symplectic integrators are specifically designed to preserve the geometric structure of Hamiltonian systems, making them more stable over longer times, particularly for systems where conserving energy is crucial (Baker & Blackburn, 2005). Specifically, use cases for semi-implicit Euler are found in physics systems such as orbital mechanics or molecular dynamics (Hernandez & Bertschinger, 2015) .

2.4.3 Leapfrog

Leapfrog integration is a second-order method that updates velocity and position at varying time-steps. The velocity is being calculated at half-steps in contrast to the position. This staggered approach of iterating both variables causes them to "leapfrog" over each other, hence the naming scheme.

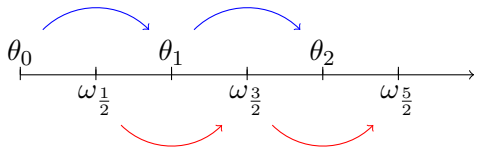

Note that the stability of this integrator is dependent on the time-step satisfying, $\Delta t \in \mathbb{R}_{>0}$ such that $\Delta t < \frac{2}{\omega}$. In general, if we consider a differential equation of the form,

$$\ddot{\theta} = F(\theta),$$

then the leapfrog integration method consists of the following steps during a single iteration,

$$\omega_{\frac{n+1}{2}} = \omega_{\frac{n-1}{2}} + F(\theta)\Delta t \tag{1}$$

$$\theta_{n+1} = \theta_n + \omega_{\frac{n+1}{2}}\Delta t \tag{2}$$

2.4.4 Runge-Kutta

Runge-Kutta are a family of iterative methods for solving ODEs numerically. They provide high accuracy while maintaining explicit formulations. The general form for a single-step Runge-Kutta method is:

$$y_{n+1} = y_n + h\sum_{i=1}^{s} b_i k_i,$$

where k_i are intermediate slopes calculated as:

$$k_i = f\left(t_n + c_i h, y_n + h\sum_{j=1}^{i-1} a_{ij}k_j\right),$$

and h is the step size.
The most common variant, and the one that we will be using for our experiments, is the fourth-order Runge-Kutta method (RK4):

$$y_{n+1} = y_n + \frac{h}{6}\left(k_1 + 2k_2 + 2k_3 + k_4\right),$$

with:

$$\begin{aligned}
k_1 &= f(t_n, y_n),\\
k_2 &= f\left(t_n + \frac{h}{2}, y_n + \frac{h}{2}k_1\right),\\
k_3 &= f\left(t_n + \frac{h}{2}, y_n + \frac{h}{2}k_2\right),\\
k_4 &= f(t_n + h, y_n + hk_3.
\end{aligned}$$

2.4.5 Gauss-Legendre Runge-Kuta

Gauss-Legendre methods are in the family of Runge-Kutta methods, however they are implicit. Moreover, they are based on Gaussian quadrature points, which ensure high accuracy and A-stability. For the Gauss-Legendre Runge-Kutta method of order 4 (GLRK4), the Butcher tableau is constructed using two collocation points in the interval $[0, 1]$, which provides fourth-order accuracy.
The method involves solving for intermediate stages k_1 and k_2 using:

$$k_1 = f\left(t_n + c_1 h, y_n + h(a_{11}k_1 + a_{12}k_2)\right),$$
$$k_2 = f\left(t_n + c_2 h, y_n + h(a_{21}k_1 + a_{22}k_2)\right),$$

where the coefficients a_{ij}, b_i, and c_i come from Gaussian quadrature. These coefficients are:

$$\text{Stages:} \quad c_1 = \frac{1}{2} - \frac{\sqrt{3}}{6}, \quad c_2 = \frac{1}{2} + \frac{\sqrt{3}}{6},$$

$$\text{Weights:} \quad b_1 = \frac{1}{2}, \quad b_2 = \frac{1}{2},$$

$$\text{Matrix:} \quad \begin{bmatrix} a_{11} & a_{12} \\ a_{21} & a_{22} \end{bmatrix} = \begin{bmatrix} \frac{1}{4} & \frac{1}{4} - \frac{\sqrt{3}}{6} \\ \frac{1}{4} + \frac{\sqrt{3}}{6} & \frac{1}{4} \end{bmatrix}.$$

Then, the final update is given by:

$$y_{n+1} = y_n + h \sum_{i=1}^{2} b_i k_i.$$

3 Simple Pendulum

3.1 History and Motivations

The simple pendulum has a rich history, spanning several centuries with a variety of uses. Although pendulums have been utilized since ancient times, their analytical study only began in the early modern period by Galileo (Baker & Blackburn, 2005). In the 16th century, the first pendulum clock was invented. This clock, using a pendulum for timekeeping, was far more accurate than its mechanical counterparts (Tirapicos, 2024).

Pendulums were also found to be crucial in measuring gravitational acceleration and played a significant role in improving the precision of scientific measurements, particularly with the development of Henry Kater's pendulum in 1817 (Pettersen, 2016).

The pendulum's simple yet influential dynamics have provided valuable insights into physics and engineering, making it an enduring object of study and application.

3.2 Equations of Motion and Characteristics

We derive the characteristics of the simple pendulum from the following ODE where g represents the gravitational constant, l denotes the pendulum's arm, and θ is the angular displacement of the pendulum's arm from the rest position (Baker & Blackburn, 2005):

$$\ddot{\theta} = -\frac{g}{l} \sin\theta$$

By introducing a new variable such as $\omega = \dot{\theta}$ denoting angular velocity, we can express the system of equations for a simple pendulum as:

$$\begin{cases} \dot{\theta} = \omega \\ \dot{\omega} = -\frac{g}{l} \sin\theta \end{cases}$$

We begin by finding the fixed points of the system by setting both equations to zero and determining the values that satisfy the equations:

$$\dot{\theta} = \dot{\omega} = 0 \implies \begin{cases} \omega = 0 \\ \theta = n\pi, \quad n \in \mathbb{Z} \end{cases}$$

Thus, we have found two fixed points at the top and bottom of the range for a pendulum's swing:

$$(2n\pi, 0), \quad ((2n+1)\pi, 0), \quad n \in \mathbb{Z}$$

To avoid redundancy, we will only analyze the fixed points for $n = 0$. First, we evaluate the stability of the linear system using its Jacobian:

$$J = \begin{bmatrix} \frac{\partial \dot{\theta}}{\partial \theta} & \frac{\partial \dot{\theta}}{\partial \omega} \\ \frac{\partial \dot{\omega}}{\partial \theta} & \frac{\partial \dot{\omega}}{\partial \omega} \end{bmatrix} = \begin{bmatrix} 0 & 1 \\ -\frac{g}{l}\cos\theta & 0 \end{bmatrix}$$

Considering the fixed point $(0, 2n\pi)$:

$$J(0,0) = \begin{bmatrix} 0 & 1 \\ -\frac{g}{l} & 0 \end{bmatrix}$$

We compute the eigenvalues of the linearized system:

$$\det \begin{bmatrix} 0-\lambda & 1 \\ -\frac{g}{l} & 0-\lambda \end{bmatrix} \implies \lambda^2 + 1 = 0 \implies \lambda = \pm i$$

Since the real part of the eigenvalues is zero, we have concluded that the first fixed point $(2n\pi, 0)$ is a center, hence Lyapunov stable.

Next, we analyze the fixed point $((2n+1)\pi, 0)$:

$$J(\pi, 0) = \begin{bmatrix} 0 & 1 \\ \frac{g}{l} & 0 \end{bmatrix}$$

Again, we find the eigenvalues of the linearized system

$$\det \begin{bmatrix} 0-\lambda & 1 \\ \frac{g}{l} & 0-\lambda \end{bmatrix} \implies \lambda^2 - 1 = 0 \implies \lambda_1 = -1, \quad \lambda_2 = 1$$

Since $\lambda_1 < 0 < \lambda_2$, we conclude that the second fixed point $((2n+1)\pi), 0$ is a saddle, hence not Lyapunov stable.

Now we examine the orbital behavior of a simple pendulum. To do this, we approximate the region as a disc, asthe orbits are not perfectly circular, as can be seen in the phase portrait of a simple pendulum (Figure 1). First, we show existence of periodic orbits within the disc D_l of radius l, where $\theta \in (-\pi, \pi)$ (i.e., one full oscillation cycle). We show that D_l satisfies the following conditions:

- **Closed:**
  - The phase space of the simple pendulum is defined by the pair (θ, ω), where $\theta \in (-\pi, \pi)$ and $\omega \in \mathbb{R}$. Therefore, the region $D_l = \{(\theta, \omega) \mid -\pi < \theta < \pi \text{ and } \omega \in \mathbb{R}\}$ is closed because it includes the boundary values of θ and encompasses the possible values of ω.
- **Bounded:**
  - In a subsequent section, we demonstrate that the total energy of the simple pendulum is conserved. Due to this fact, it is evident that D_l is bounded.

- **Positively invariant:**
  - For the region D_l to be positively invariant, it must be shown that if the trajectory starts in the region D_l, it will remain inside D_l for all future times. Since both equations in the system are bounded, with θ oscillating between $-\pi$ and π and $\dot{\omega} = -\frac{g}{l}\sin\theta$, where $\sin\theta$ is bounded between 1 and 1, the trajectory remains within the region D_l and is positively invariant.
- **There exists no fixed points:**
  - As determined earlier, the only fixed point in the phase space lies at $(0, 0)$. Thus we restrict the region where periodic orbits may lie to exclude the origin.

By applying the Poincaré-Bendixson Theorem (the first three criteria) and demonstrating the absence of fixed points in D_l, we can conclude that periodic orbits exist within in this region. This behavior may also be seen clearly from the center nature of the fixed point at $(0, 0)$. These periodic orbits correspond to the periodic swing of the pendulum.

Next, we discuss the second type of orbit of the simple pendulum less formally. There are two homoclinic orbits between the fixed points, where the mass approaches either fixed point in infinite time (commonly referred to as the separatrix). We can describe this behavior by defining the ω and α sets of this orbit

$$\omega(\phi) = \{(\pi, 0)\} \quad \text{or} \quad \{(-\pi, 0)\}$$
$$\alpha(\phi) = \{(-\pi, 0)\} \quad \text{or} \quad \{(\pi, 0)\}$$

To summarize, we have explored the dynamics of the simple pendulum through its governing ODEs. By examining the fixed points, we identified a stable center at the equilibrium position and an unstable saddle at the inverted position of a simple pendulum. We also demonstrated the existence of periodic orbits within the bounded region D_l, with the Poincaré-Bendixson Theorem confirming their periodic nature. Furthermore, the separatrix behavior was described by the homoclinic orbits connecting the two fixed points. Thereby we have revealed the oscillatory nature of the simple pendulum.

3.3 Hamiltonian Mechanics for Simple Pendulum

We begin by considering the simplified dynamic system for a simple pendulum, given by the following equations (Hairer, Wanner & Lubich, 2006):

$$\begin{cases} \dot{p} = q \\ \dot{q} = -\sin p \end{cases}$$

The energy function for a 2-dimensional system can be derived from the second-order equation $\ddot{p} = -u'(p)$, resulting in the system:

$$\begin{cases} \dot{p} = q \\ \dot{q} = -u'(p) \end{cases}$$

Where the total energy E of the system is the sum of the kinetic and potential energies

$$E = E_k + E_p$$
$$E = \frac{1}{2}p^2 + u(x)$$

Solving for potential energy, we find $u(p) = (1 - \cos p)$, leading to the Hamiltonian:

$$H(p, q) = \frac{1}{2}q^2 + (1 - \cos p)$$

The Hamiltonian system is thus expressed in the form:

$$\begin{cases} \dot{p} = \frac{\partial H}{\partial q} \\ \dot{q} = -\frac{\partial H}{\partial p} \end{cases}$$

After solving, we are found to be left with the starting dynamical system.

Next, we show that energy is conserved by computing the time derivative of the total energy. Using the Hamiltonian derived, we have:

$$\begin{aligned} \frac{d}{dt}H(\phi^t(p_0, q_0)) &= \frac{d}{dt}H(p(t), q(t)), \\ &= p(t)\dot{p}(t) + \dot{q}(t)\sin(p(t)), \\ &= -q(t)\sin(p(t)) + \sin(p(t))q(t), \\ &= 0. \end{aligned}$$

Thus, using the energy method, we have shown that energy is conserved for a simple pendulum. However, we will find that replicating this energy conservation trait in numerical simulations using various integration methods for simple pendulums can be difficult in subsequent analyses.

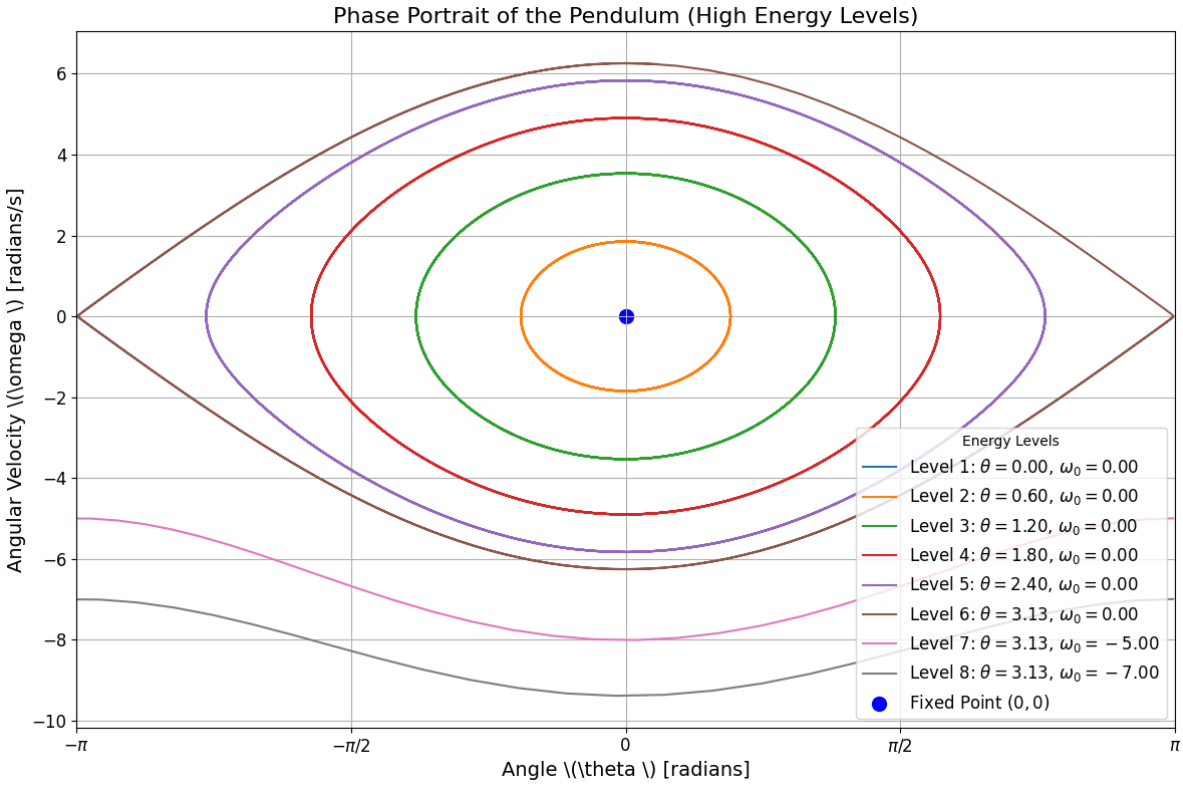

Figure 1: Phase Portrait of a Simple Pendulum at various energy levels

3.4 Integration Methods

3.4.1 Explicit Euler

Implementing the explicit Euler integration method for a simple pendulum is straightforward using the methodology discussed earlier, we derive the system following system to simulate the

movement of the simple pendulum:

$$\theta_{n+1} = \theta_n + \Delta t \cdot \omega_n$$
$$\omega_{n+1} = \omega_n + \Delta t \cdot -\frac{g}{l} \sin \theta_n$$

In this system, the angular acceleration at time-step n is given by $\dot{\omega} = -\frac{g}{l} \sin \theta_n$, which is from the pair of ODEs derived earlier.

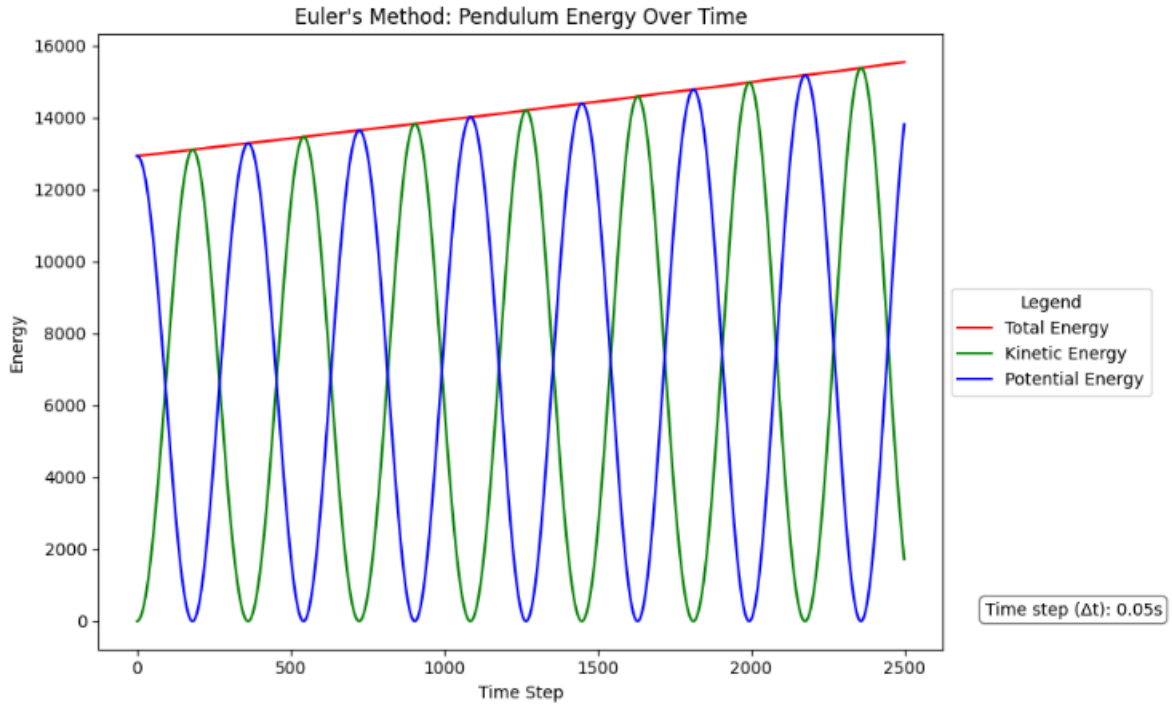

Figure 2: Energy of a Simple Pendulum using Explicit Euler

One notable characteristic of using the explicit Euler method to simulate a simple pendulum is that the total energy constantly accumulates over time, as shown in Figure 2. This accumulation occurs due to errors in the integration method. As a result, the explicit Euler method violates a key characteristic of simple pendulums found earlier, where energy is conserved, leading to deviations from the true solution.

3.4.2 Semi-Implicit Euler

Implementing the semi-implicit Euler integration method is a bit more complex, as it requires first calculating the angular velocity at the next time step before updating the position. The method is represented by the following system:

$$\omega_{n+1} = \omega_n + \Delta t \cdot -\frac{g}{l} \sin \theta_n$$
$$\theta_{n+1} = \theta_n + \Delta t \cdot \omega_{n+1}$$

While an improvement to the explicit Euler integration method, it still does not conserve total energy. However, the total energy remains bounded, though not tightly as seen in Figure 3. Future integration methods discussed aim to tighten the bound on total energy.

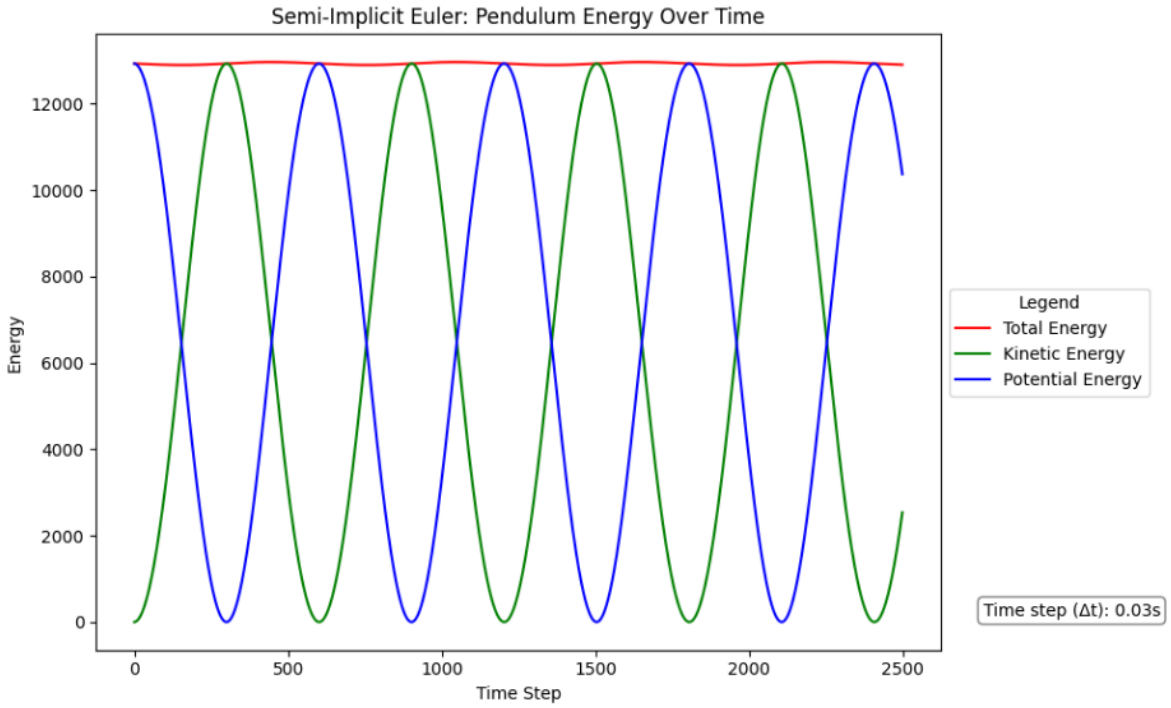

Figure 3: Energy of a Simple Pendulum using semi-implicit Euler

3.4.3 Leapfrog

Due to the second-order nature of the Leapfrog integration method, it is more stable for the oscillatory motion of the simple pendulum. For our purposes we maintained a small enough time-step ($\Delta t = 0.03$) during our simulations. Indeed, Leapfrog was relatively stable for the behaviour of the system. We have outlined the iteration process specific to the simple pendulum below,

$$\omega_{\frac{n+1}{2}} = \omega_{\frac{n-1}{2}} - \frac{g}{L}\sin(\theta_n)\Delta t \tag{3}$$

$$\theta_{n+1} = \theta_n + \omega_{\frac{n+1}{2}}\Delta t \tag{4}$$

3.4.4 Runge-Kutta

Let $\mathbf{y} = (\theta, \omega)$ represent the state vector. The RK4 update for $\mathbf{y}$ is:

$$\mathbf{y}_{n+1} = \mathbf{y}_n + \frac{h}{6}\left(\mathbf{k}_1 + 2\mathbf{k}_2 + 2\mathbf{k}_3 + \mathbf{k}_4\right),$$

where the stages $\mathbf{k}_i$ are computed as:

$$\begin{aligned}
\mathbf{k}_1 &= \mathbf{f}(t_n, \mathbf{y}_n), \\
\mathbf{k}_2 &= \mathbf{f}\left(t_n + \frac{h}{2}, \mathbf{y}_n + \frac{h}{2}\mathbf{k}_1\right), \\
\mathbf{k}_3 &= \mathbf{f}\left(t_n + \frac{h}{2}, \mathbf{y}_n + \frac{h}{2}\mathbf{k}_2\right), \\
\mathbf{k}_4 &= \mathbf{f}\left(t_n + h, \mathbf{y}_n + h\mathbf{k}_3\right).
\end{aligned}$$

Here, $\mathbf{f}(t, \mathbf{y})$ represents the system of ODEs:

$$\mathbf{f}(t, \mathbf{y}) = \begin{bmatrix} \omega \\ -\frac{g}{L}\sin(\theta) \end{bmatrix}.$$

This algorithm iteratively updates θ and ω at each time step h to simulate the pendulum's motion.

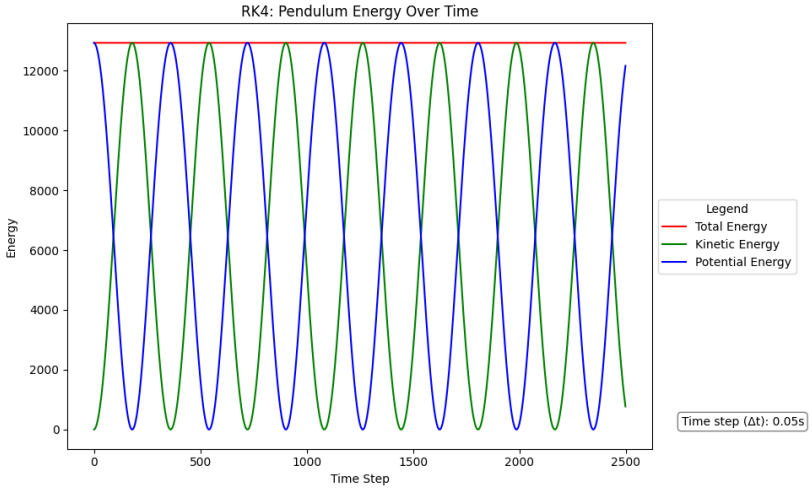

Figure 4: Runge-Kutta on a Single Pendulum

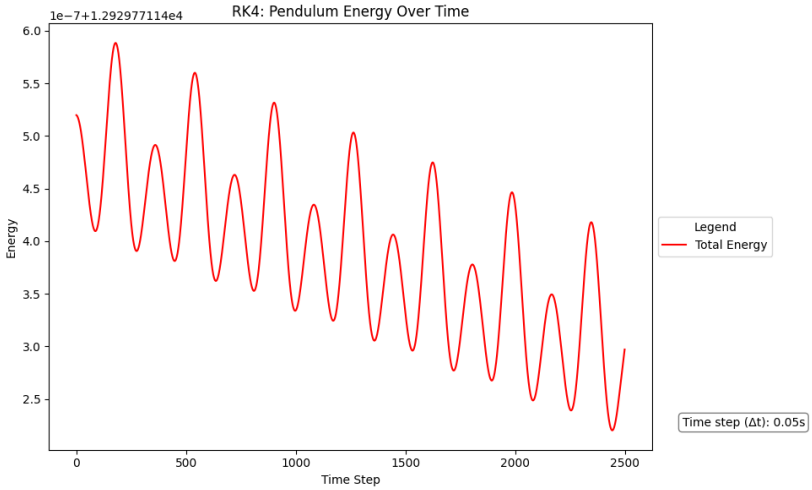

Figure 5: Runge-Kutta is not Symplectic

3.4.5 Gauss-Legendre Runge-Kutta

$$\dot{\theta} = \omega, \quad \dot{\omega} = -\frac{g}{L}\sin(\theta),$$

with the state vector $\mathbf{y} = (\theta, \omega)$. The implicit updates involve solving for intermediate stages $\mathbf{k}_1$ and $\mathbf{k}_2$ using:

$$\mathbf{k}_1 = \mathbf{f}\left(t_n + c_1 h, \mathbf{y}_n + h(a_{11}\mathbf{k}_1 + a_{12}\mathbf{k}_2)\right),$$
$$\mathbf{k}_2 = \mathbf{f}\left(t_n + c_2 h, \mathbf{y}_n + h(a_{21}\mathbf{k}_1 + a_{22}\mathbf{k}_2)\right),$$

where $\mathbf{f}(t, \mathbf{y})$ is the same as before:

$$\mathbf{f}(t, \mathbf{y}) = \begin{bmatrix} \omega \\ -\frac{g}{L}\sin(\theta) \end{bmatrix}.$$

The final update is:

$$\mathbf{y}_{n+1} = \mathbf{y}_n + h \sum_{i=1}^{2} b_i \mathbf{k}_i,$$

where a_{ij}, b_i, and c_i are the Gauss-Legendre coefficients, as listed earlier. We solved the implicit equations at every step, using fsolve for its speed and accuracy. As you can see below, the oscillations are extremely small, thus the energy is bounded well.

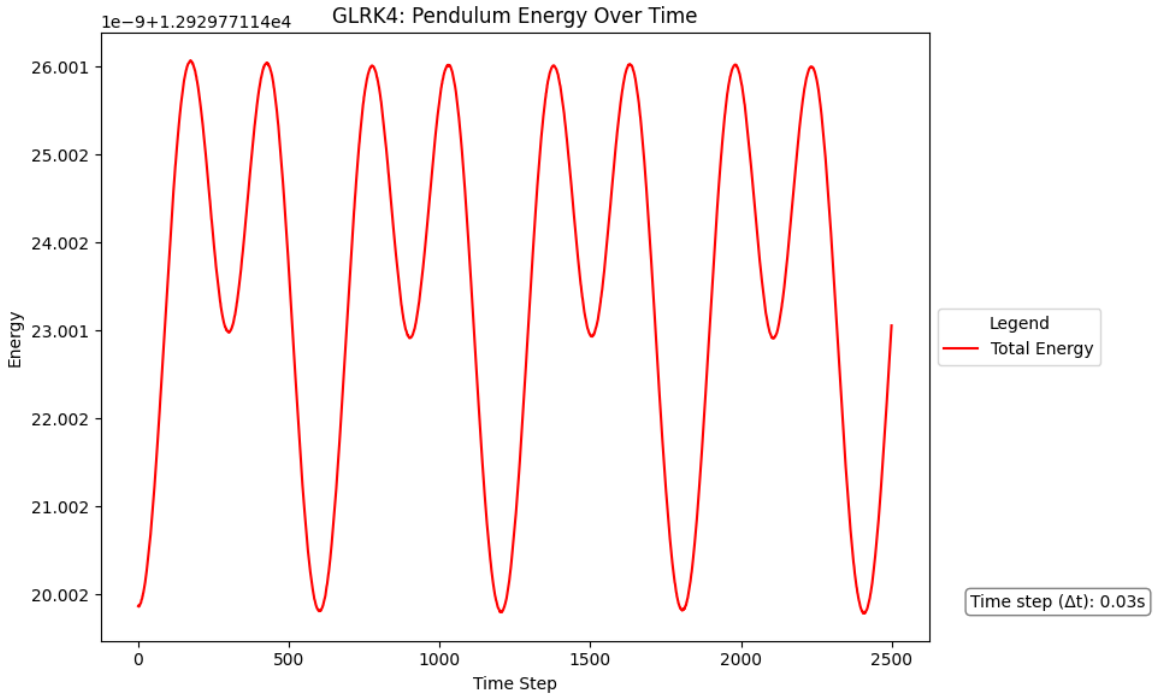

Figure 6: GLRK4 Pendulum Energy

4 Double Pendulum

4.1 History and Motivation

Accurately modeling the behaviour of a double pendulum system has been achieved only recently, thus, its history is rather brief in comparison to the simple pendulum. However, the study of the double pendulum has brought forth many applications in fields such as robotics [Graichen, Treuer, and Zeitz 2007] and biomechanics [Betzler et al. 2008]. This dynamical system is a classical example of chaos. We will discuss the oscillatory behaviour of the double pendulum in a non-damping environment, and subsequently consider how shifts in energy lead to unpredictable motion. In our study, we will apply each of our chosen symplectic integrators and analyze how the chaotic behaviour of the double pendulum affects the performance of each integration method.

4.2 Equations of Motion and Characteristics

For our purposes, we assume the rods connecting masses are weightless and rigid, with lengths L_1 and L_2. Additionally, we assume that there is no friction present in the pivots. To construct

the ODEs for the double pendulum we consider the coordinates of each mass (m_1, m_2),

$$x_1 = L_1 \sin(\theta_1), \tag{5}$$
$$y_1 = -L_1 \cos(\theta_1), \tag{6}$$
$$x_2 = x_1 + L_2 \sin(\theta_2), \tag{7}$$
$$y_2 = -y_1 - L_2 \cos(\theta_2), \tag{8}$$

where θ_1 and θ_2 correspond to the angles relative to the resting position of the first and second rods, respectively. In addition, we can observe that x_2 depends on x_1 and y_2 depends on y_1, indicating the non-linear dynamics of this system. It follows that the kinetic (K) and potential (P) energies are of the forms,

$$K = \frac{m_1(\dot{x}_1^2 + \dot{y}_1^2)}{2} + \frac{m_2(\dot{x}_2^2 + \dot{y}_2^2)}{2},$$
$$P = m_1 g y_1 + m_2 g y_2.$$

Substituting our equations x_1, x_2, y_1, y_2 we have that,

$$K = \frac{(m_1 + m_2)}{2} L_1^2 \dot{\theta}_1^2 + \frac{m_2}{2} L_2^2 \dot{\theta}_2^2 + m_2 L_1 L_2 \cos(\theta_1 - \theta_2)\dot{\theta}_1 \dot{\theta}_2, \tag{9}$$
$$P = -m_1 g L_1 \cos(\theta_1) - m_2 g[L_1 \cos(\theta_1) + L_2 \cos(\theta_2)]. \tag{10}$$

Hence, the Lagrangian $L = K - P$ is of the form,

$$\begin{aligned} L = \frac{(m_1 + m_2)}{2} L_1^2 \dot{\theta}_1^2 + \frac{m_2}{2} L_2^2 \dot{\theta}_2^2 + m_2 L_1 L_2 \cos(\theta_1 - \theta_2)\dot{\theta}_1 \dot{\theta}_2 \\ + (m_1 + m_2) g L_1 \cos(\theta_1) + m_2 g L_2 \cos(\theta_2). \end{aligned} \tag{11}$$

We can now write the Lagrangian equations $\frac{\partial L}{\partial \theta_i} - \frac{d}{dt}\frac{\partial L}{\partial \dot{\theta}_i} = 0$ for $i \in \{1, 2\}$,

$$(m_1 + m_2) L_1 \ddot{\theta}_1 + m_2 L_2 \ddot{\theta}_2 \cos(\theta_1 - \theta_2) + m_2 L_2 \dot{\theta}_1^2 \sin(\theta_1 - \theta_2) + (m_1 + m_2) g \sin(\theta_1) = 0, \tag{12}$$
$$L_2 \ddot{\theta}_2 + L_1 \ddot{\theta}_1 \cos(\theta_1 - \theta_2) - L_1 \dot{\theta}_1^2 \sin(\theta_1 - \theta_2) + g \sin(\theta_2) = 0. \tag{13}$$

Dividing (8) by $(m_1 + m_2)L_1$, and dividing (9) by L_2, we have that

$$\ddot{\theta}_1 + \xi_1(\theta_1, \theta_2)\ddot{\theta}_2 = F_2(\theta_1, \theta_2, \dot{\theta}_1, \dot{\theta}_2), \tag{14}$$
$$\ddot{\theta}_2 + \xi_2(\theta_1, \theta_2)\ddot{\theta}_1 = F_2(\theta_1, \theta_2, \dot{\theta}_1, \dot{\theta}_2), \tag{15}$$

where,

$$\xi_1(\theta_1, \theta_2) = (\frac{m_2}{m_1 + m_2})\frac{L_2}{L_1} \cos(\theta_1 - \theta_2), \tag{16}$$
$$\xi_2(\theta_1, \theta_2) = \frac{L_1}{L_2} \cos(\theta_1 - \theta_2), \tag{17}$$
$$F_1(\theta_1, \theta_2, \dot{\theta}_1, \dot{\theta}_2) = -(\frac{m_2}{m_1 + m_2})\frac{L_1}{L_2}\dot{\theta}_2^2 \sin(\theta_1 - \theta_2) - \frac{g}{L_1}\sin(\theta_1), \tag{18}$$
$$F_2(\theta_1, \theta_2, \dot{\theta}_1, \dot{\theta}_2) = \frac{L_1}{L_2}\dot{\theta}_1^2 \sin(\theta_1 - \theta_2) - \frac{g}{L_2}\sin(\theta_2). \tag{19}$$

We can rewrite (14) and (15) using matrix notation as,

$$\begin{pmatrix} 1 & \xi_1 \\ \xi_2 & 1 \end{pmatrix} \begin{pmatrix} \ddot{\theta}_1 \\ \ddot{\theta}_2 \end{pmatrix} = \begin{pmatrix} F_1 \\ F_2 \end{pmatrix} \implies \begin{pmatrix} \ddot{\theta}_1 \\ \ddot{\theta}_2 \end{pmatrix} = \frac{1}{1 - \xi_1 \xi_2} \begin{pmatrix} 1 & -\xi_1 \\ -\xi_2 & 1 \end{pmatrix} \begin{pmatrix} F_1 \\ F_2 \end{pmatrix} \tag{20}$$
$$\implies \begin{pmatrix} \ddot{\theta}_1 \\ \ddot{\theta}_2 \end{pmatrix} = \frac{1}{1 - \xi_1 \xi_2} \begin{pmatrix} F_1 - \xi_1 F_2 \\ -\xi_2 F_1 + F_2 \end{pmatrix} \tag{21}$$

Now, we introduce a change of variables in order to convert the system of second-order equations (21), to first-order equations. Let $\omega_1 = \dot{\theta}_1$ and $\omega_2 = \dot{\theta}_2$, then,

$$\dot{\theta}_1 = \omega_1, \tag{22}$$

$$\dot{\theta}_2 = \omega_2, \tag{23}$$

$$\dot{\omega}_1 = \frac{F_1 - \xi_1 F_2}{1 - \xi_1 \xi_2}, \tag{24}$$

$$\dot{\omega}_2 = \frac{-\xi_2 F_1 + F_2}{1 - \xi_1 \xi_2}. \tag{25}$$

4.3 Hamiltonian Mechanics for Double Pendulum

In order to transition from the Lagrangian (11) to Hamiltonian mechanics, we can use the Legendre transformation of the form,

$$H = \dot{\theta}_1 \frac{\partial L}{\partial \dot{\theta}_1} + \dot{\theta}_2 \frac{\partial L}{\partial \dot{\theta}_2} - L, \tag{26}$$

where H is the Hamiltonian of the system. Let $p_i = \frac{\partial L}{\partial \dot{\theta}_i}$, for $i \in \{1, 2\}$, be the momenta. Then, the Legendre transformation yields the following system of equations,

$$\dot{\theta}_i = \frac{\partial H}{\partial p_i}, \tag{27}$$

$$\dot{p}_i = -\frac{\partial H}{\partial \theta_i}. \tag{28}$$

Finally, we can write the Hamilton's canonical equations in the form,

$$\dot{\theta}_1 = \frac{p_1 L_2 - p_2 L_2 \cos(\theta_1 - \theta_2)}{L_1^2 L_2 [m_1 + m_2 \sin^2(\theta_1 - \theta_2)]}, \tag{29}$$

$$\dot{\theta}_2 = \frac{p_2 (m_1 + m_2) L_1 - p_1 m_2 L_2 \cos(\theta_1 - \theta_2)}{m_2 L_1 L_2^2 [m_1 + m_2 \sin^2(\theta_1 - \theta_2)]}, \tag{30}$$

$$\dot{p}_1 = -(m_1 + m_2) g L_1 \sin(\theta_1) - \gamma_1 + \gamma_2, \tag{31}$$

$$\dot{p}_2 = -m_2 g L_2 \sin(\theta_2) + \gamma_1 - \gamma_2, \tag{32}$$

where,

$$\gamma_1 = \frac{p_1 p_2 \sin(\theta_1 - \theta_2)}{L_1 L_2 [m_1 + m_2 \sin^2(\theta_1 - \theta_2)]}, \tag{33}$$

$$\gamma_2 = \frac{\sin[2(\theta_1 - \theta_2)][p_1^2 m_2 L_2^2 - 2 p_1 p_2 m_2 L_1 L_2 \cos(\theta_1 - \theta_2) + p_2^2 (m_1 + m_2) L_1^2]}{2 L_1^2 L_2^2 [m_1 + m_2 \sin^2(\theta_1 - \theta_2)]^2}. \tag{34}$$

Now, we have obtained a system of differential equations of the first-order which depend on the angles θ_1 and θ_2, as well as the momenta p_1 and p_2. Naturally, this numerical model of the dynamical system allows for our numerical analysis. We can apply the symplectic Runge-Kutta method to further simplify our Hamiltonian.

4.4 Chaotic and Oscillatory Nature

First, we will consider the behaviour of the double pendulum system when the initial angle of displacement is relatively small. Using the Lagrangian (11) that we obtained in the previous section, we can approximate the following terms by expansion of its Maclaurin series, for small values of θ_1 and θ_2,

$$\cos(\theta_1) \approx 1 - \frac{\theta_1^2}{2} \qquad \cos(\theta_2) \approx 1 - \frac{\theta_2^2}{2} \qquad \cos(\theta_1 - \theta_2) \approx 1 - \frac{(\theta_1 - \theta_2)^2}{2} \approx 1$$

Note that $(\theta_1 - \theta_2)^2 = \theta_1^2 - 2\theta_1\theta_2 + \theta_2^2$. So, for particularly small values of θ_1 and θ_2,

$$\theta_1^2 + \theta_2^2 \approx 2\theta_1\theta_2 \implies (\theta_1 - \theta_2)^2 \approx 0$$

Now, substituting our approximations back into the Lagrangian (11), we have that,

$$L = \frac{(m_1 + m_2)}{2} L_1^2 \dot{\theta}_1^2 + \frac{m_2}{2} L_2^2 \dot{\theta}_2^2 + m_2 L_1 L_2 \dot{\theta}_1 \dot{\theta}_2 + \frac{(m_1 + m_2)}{2} g L_1 \theta_1^2 + \frac{m_2}{2} g L_2 \theta_2^2. \tag{35}$$

Once more, we compute the Lagrangian equations to obtain,

$$(1 + \frac{m_1}{m_2}) L_1 \ddot{\theta}_1 + L_2 \ddot{\theta}_2 + (1 + \frac{m_1}{m_2}) g \theta_1 = 0, \tag{36}$$

$$L_1 \ddot{\theta}_1 + L_2 \ddot{\theta}_2 + g\theta_2 = 0. \tag{37}$$

Undergoing the same matrix operations and change in variables, letting $\omega_1 = \dot{\theta}_1$ and $\omega_2 = \dot{\theta}_2$, we have the system,

$$\dot{\theta}_1 = \omega_1, \tag{38}$$

$$\dot{\theta}_2 = \omega_2, \tag{39}$$

$$\dot{\omega}_1 = \frac{\Gamma_1 - \eta_1 \Gamma_2}{1 - \eta_1 \eta_2}, \tag{40}$$

$$\dot{\omega}_2 = \frac{-\eta_2 \Gamma_1 + \Gamma_2}{1 - \eta_1 \eta_2}, \tag{41}$$

where,

$$\Gamma_1(\theta_1) = -\frac{g}{L_1}\theta_1, \tag{42}$$

$$\Gamma_2(\theta_2) = -\frac{g}{L_2}\theta_2, \tag{43}$$

$$\eta_1 = \frac{L_2}{1 - L_1(1 + \frac{m_1}{m_2})}, \tag{44}$$

$$\eta_2 = \frac{L_1}{L_2}. \tag{45}$$

Observe the similarities between the equations describing the motion of a simple pendulum system, and equations (42) and (43). In particular, $\sin(\theta_i) \approx \theta_i$ for small values of θ_i. Moreover, this system of equations is linear, unlike the second-order system we derived in section 4.2. During our simulations, we noticed the oscillatory behaviour of both pendulums to be reminiscent of the simple pendulum. For small initial values of θ_1 and θ_2, we saw a relatively fixed period preserved throughout the simulation (i.e. no chaos was observed). These observations seemingly agree with our derived linear system of equations describing the motion of a double pendulum for small initial displacements. In general, however, as the initial values for θ_1 and θ_2 increase, we require a more nuanced approach in order to predict the systems oscillatory behaviour (e.g. use the derived Hamiltonian system (29)-(32) for numerical analysis). In our simulations, minor perturbations to the initial conditions resulted in radically different, and unpredictable motion. All parameters (e.g. angular velocity, position, period, etc.) were affected by these small changes, and some integration methods failed to effectively capture the behaviour due to chaos.

4.5 Phase Portrait

In Fig. 1 and 2, we show the phase portraits of the first and second arms of the double pendulum, respectively. Changes to the initial conditions, such as angular velocity and the position, will greatly alter the generated phase portrait. In particular, as the amount of energy introduced into the system increases, there is more irregularity in the dynamics of the system. This result is more pronounced in the phase portrait of the second arm, where we see a larger scale for both angular velocity and position.

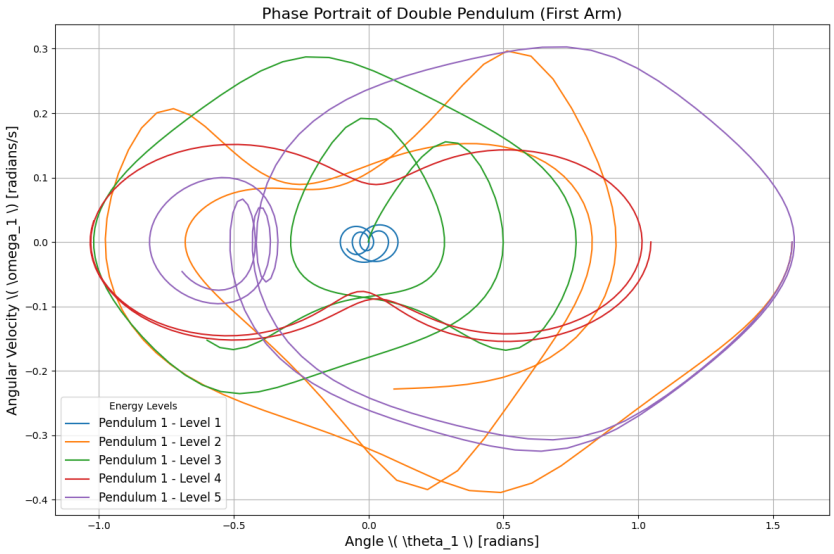

Figure 7: Double Pendulum Phase Portrait, First Arm

Figure 8: Double Pendulum Phase Portrait, Second Arm

4.6 Integration Methods

4.6.1 Explicit Euler

We now apply the explicit Euler method to the system of equations for a double pendulum, which is given by the following equations (Baker & Blackburn, 2005):

$$\theta_1^{n+1} = \theta_1^n + \Delta t \cdot \omega_1^n,$$
$$\theta_2^{n+1} = \theta_2^n + \Delta t \cdot \omega_2^n,$$
$$\omega_1^{n+1} = \omega_1^n + \Delta t \cdot \frac{-g(2m_1+m_2)\sin\theta_1^n - m_2 g \sin(\theta_1^n - 2\theta_2^n) - 2\sin(\theta_1^n-\theta_2^n)m_2\left((\omega_2^n)^2 l_2 + (\omega_1^n)^2 l_1 \cos(\theta_1^n-\theta_2^n)\right)}{l_1\left(2m_1+m_2-m_2\cos^2(\theta_1^n-\theta_2^n)\right)},$$
$$\omega_2^{n+1} = \omega_2^n + \Delta t \cdot \frac{2\sin(\theta_1^n-\theta_2^n)\left((\omega_1^n)^2 l_1(m_1+m_2) + g(m_1+m_2)\cos\theta_1^n + (\omega_2^n)^2 l_2 m_2 \cos(\theta_1^n-\theta_2^n)\right)}{l_2\left(2m_1+m_2-m_2\cos^2(\theta_1^n-\theta_2^n)\right)}.$$

Using explicit Euler to simulate the double pendulum, we observe in Figure 4 that total energy still accumulates over time due to errors in the integration method. However, in contrast to simulations for the simple pendulum, the error is not consistent reflecting the chaotic nature of the double pendulum system.

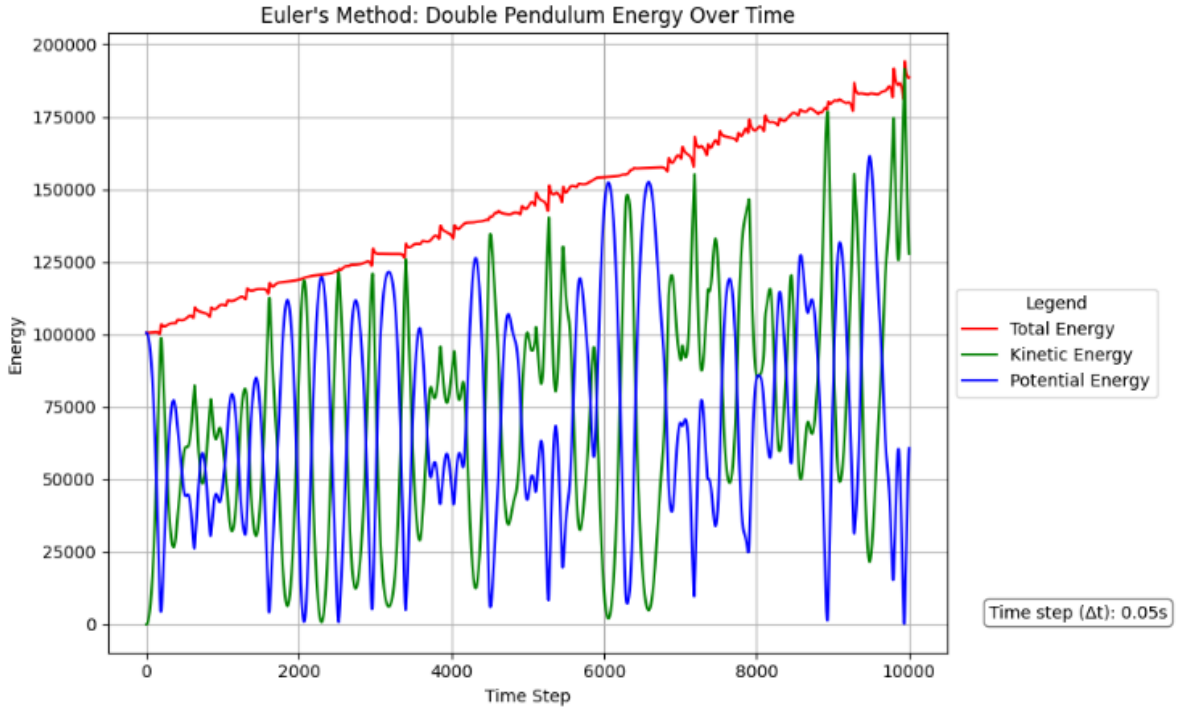

Figure 9: Energy of a Double Pendulum using Explicit Euler

4.6.2 Semi-Implicit Euler

Once again an improvement from the explicit Euler integration method, we apply the same semi-implicit Euler method to the system of equations for the double pendulum:

$$\theta_1^{n+1} = \theta_1^n + \Delta t \cdot \omega_1^{n+1},$$
$$\theta_2^{n+1} = \theta_2^n + \Delta t \cdot \omega_2^{n+1},$$
$$\omega_1^{n+1} = \omega_1^n + \Delta t \cdot \frac{-g(2m_1+m_2)\sin\theta_1^n - m_2 g \sin(\theta_1^n - 2\theta_2^n) - 2\sin(\theta_1^n-\theta_2^n)m_2\left((\omega_2^n)^2 l_2 + (\omega_1^n)^2 l_1 \cos(\theta_1^n-\theta_2^n)\right)}{l_1\left(2m_1+m_2-m_2\cos^2(\theta_1^n-\theta_2^n)\right)},$$
$$\omega_2^{n+1} = \omega_2^n + \Delta t \cdot \frac{2\sin(\theta_1^n-\theta_2^n)\left((\omega_1^n)^2 l_1(m_1+m_2) + g(m_1+m_2)\cos\theta_1^n + (\omega_2^n)^2 l_2 m_2 \cos(\theta_1^n-\theta_2^n)\right)}{l_2\left(2m_1+m_2-m_2\cos^2(\theta_1^n-\theta_2^n)\right)}.$$

Where only calculations for the next time step of θ_1 and θ_2 differ from explicit Euler.

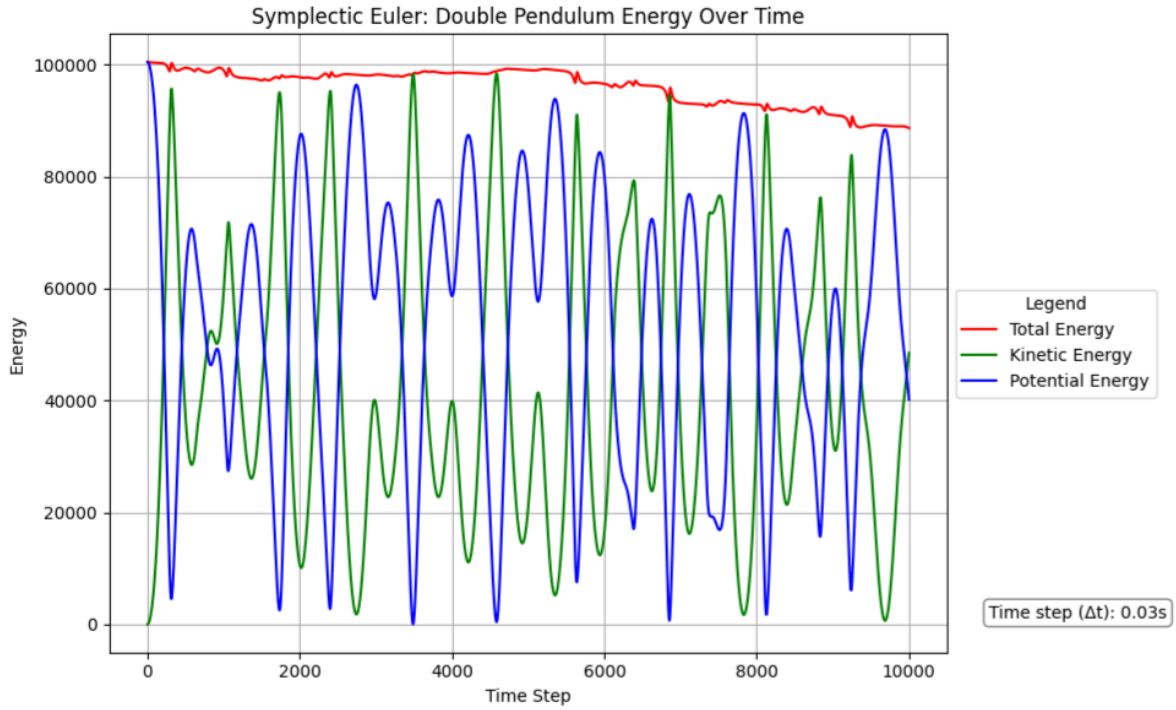

Figure 10: Energy of a Double Pendulum using Semi-implicit Euler

However, in contrast to the explicit Euler method, the total energy of the simple pendulum is no longer bounded. Instead of conserving energy as expected, the total energy dissipates over time as seen in Figure 5, highlighting the limitations of the semi-implicit Euler method in accurately modeling the dynamics of this system over long simulations.

4.6.3 Leapfrog

Even for a small time-step ($\Delta t = 0.3$), the Leapfrog integration method was neither accurate nor stable when applied to analyze its energy conservation capabilities in the context of a double pendulum system. This is likely ascribable to the second-order nature of this integration method. Below, we have the process by which a single iteration is performed,

$$\omega_{1_{\frac{n+1}{2}}} = \omega_{1_{\frac{n-1}{2}}} + \psi_1 \Delta t, \tag{46}$$

$$\omega_{2_{\frac{n+1}{2}}} = \omega_{2_{\frac{n-1}{2}}} + \psi_2 \Delta t, \tag{47}$$

$$\theta_{1_{n+1}} = \theta_{1_n} + \omega_{1_{\frac{n+1}{2}}} \Delta t, \tag{48}$$

$$\theta_{2_{n+1}} = \theta_{2_n} + \omega_{2_{\frac{n+1}{2}}} \Delta t, \tag{49}$$

where,

$$\begin{aligned} \psi_1 = \frac{-1}{L_1(2m_1 + m_2 - m_2\cos[2(\theta_1 - \theta_2)])}(2m_1 m_2 g \sin(\theta_1) + m_2 g \sin(\theta_1 - 2\theta_2) \\ +2m_2 \sin(\theta_1 - \theta_2)[L_1 \omega_{1_{\frac{n-1}{2}}}^2 \cos(\theta_1 - \theta_2) + L_2 \omega_{2_{\frac{n-1}{2}}}^2]), \end{aligned} \tag{50}$$

$$\psi_2 = \frac{2\sin(\theta_1 - \theta_2)[(m_1 + m_2)L_1 \omega_{1_{\frac{n-1}{2}}}^2 + (m_1 + m_2)g\cos(\theta_1) + m_2 L_2 \omega_{2_{\frac{n-1}{2}}}^2 \cos(\theta_1 - \theta_2)]}{L_2(2m_1 + m_2 - m_2\cos[2(\theta_1 - \theta_2)])}. \tag{51}$$

4.6.4 Runge-Kutta

We have θ_1, θ_2 and angular velocities ω_1, ω_2:

$$\dot{\theta}_1 = \omega_1, \quad \dot{\theta}_2 = \omega_2,$$

$$\dot{\omega}_1 = f_1(\theta_1, \theta_2, \omega_1, \omega_2), \quad \dot{\omega}_2 = f_2(\theta_1, \theta_2, \omega_1, \omega_2),$$

where f_1 and f_2 are nonlinear functions derived from the system's Lagrangian.

Let $\mathbf{y} = (\theta_1, \theta_2, \omega_1, \omega_2)$ represent the state vector. The RK4 method updates $\mathbf{y}$ as:

$$\mathbf{y}_{n+1} = \mathbf{y}_n + \frac{h}{6}\left(\mathbf{k}_1 + 2\mathbf{k}_2 + 2\mathbf{k}_3 + \mathbf{k}_4\right),$$

with intermediate stages computed as:

$$\begin{aligned}
\mathbf{k}_1 &= \mathbf{f}(t_n, \mathbf{y}_n), \\
\mathbf{k}_2 &= \mathbf{f}\left(t_n + \frac{h}{2}, \mathbf{y}_n + \frac{h}{2}\mathbf{k}_1\right), \\
\mathbf{k}_3 &= \mathbf{f}\left(t_n + \frac{h}{2}, \mathbf{y}_n + \frac{h}{2}\mathbf{k}_2\right), \\
\mathbf{k}_4 &= \mathbf{f}\left(t_n + h, \mathbf{y}_n + h\mathbf{k}_3\right).
\end{aligned}$$

Here, $\mathbf{f}(t, \mathbf{y})$ represents the system of ODEs, which includes trigonometric and nonlinear terms for the double pendulum's dynamics. The RK4 method updates all four variables at each h, trying to capture the motion of the double pendulum. As you can see below, the system is not symplectic, thus there is a loss in energy over time.

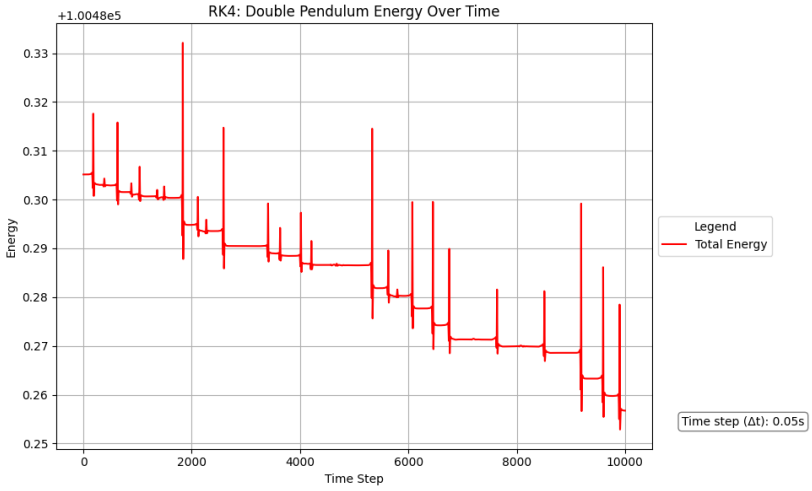

Figure 11: RK4 Double Pendulum

4.6.5 Gauss-Legendre Runge-Kutta

Again,

$$\dot{\theta}_1 = \omega_1, \quad \dot{\theta}_2 = \omega_2,$$

$$\dot{\omega}_1 = f_1(\theta_1, \theta_2, \omega_1, \omega_2), \quad \dot{\omega}_2 = f_2(\theta_1, \theta_2, \omega_1, \omega_2),$$

where f_1 and f_2 are nonlinear functions derived from the system's Lagrangian.

Let $\mathbf{y} = (\theta_1, \theta_2, \omega_1, \omega_2)$ represent the state vector. The GLRK4 method computes intermediate stages $\mathbf{k}_1$ and $\mathbf{k}_2$ using the implicit relations:

$$\mathbf{k}_1 = \mathbf{f}\left(t_n + c_1 h, \mathbf{y}_n + h(a_{11}\mathbf{k}_1 + a_{12}\mathbf{k}_2)\right),$$

$$\mathbf{k}_2 = \mathbf{f}\left(t_n + c_2 h, \mathbf{y}_n + h(a_{21}\mathbf{k}_1 + a_{22}\mathbf{k}_2)\right),$$

where c_1 and c_2 are the nodes of the Gauss-Legendre quadrature, and a_{ij} are the coefficients of the Butcher tableau for the GL-RK4 method.

Once $\mathbf{k}_1$ and $\mathbf{k}_2$ are solved, the final state $\mathbf{y}_{n+1}$ is updated as:

$$\mathbf{y}_{n+1} = \mathbf{y}_n + h \sum_{i=1}^{2} b_i \mathbf{k}_i,$$

where $b_1 = b_2 = \frac{1}{2}$ are the weights of the Gauss-Legendre quadrature.

$$\mathbf{f}(t, \mathbf{y}) = \begin{bmatrix} \omega_1 \\ \omega_2 \\ f_1(\theta_1, \theta_2, \omega_1, \omega_2) \\ f_2(\theta_1, \theta_2, \omega_1, \omega_2) \end{bmatrix}.$$

f includes the trigonometric and coupled nonlinear terms characteristic of the double pendulum dynamics. We use fsolve to solve our nonlinear equation since GLRK4 is implicit. Our results show good symplectic behavior:

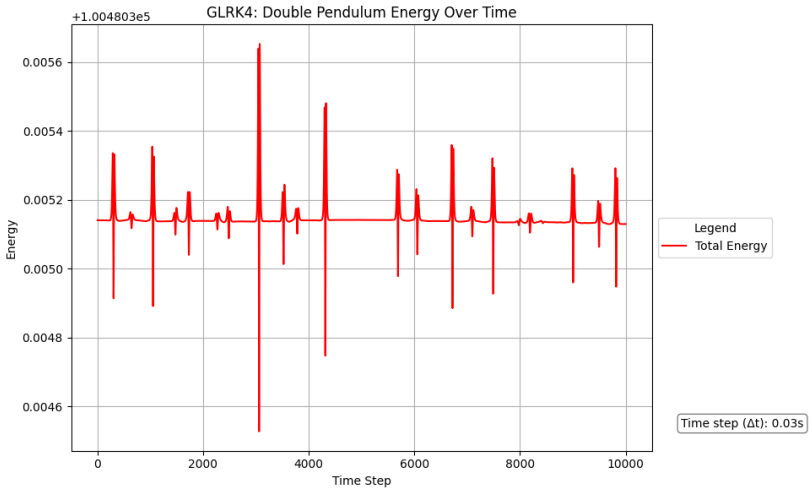

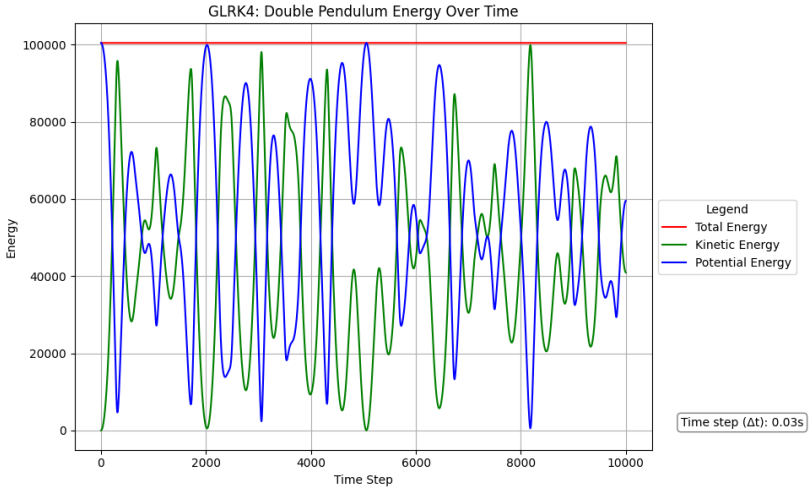

5 Results and Analysis

5.1 Simple Pendulum Results

We have explored several integration methods implemented to simulate the motion of the simple pendulum, each method with its own pros and cons.

Starting with the most intuitive to understand, the explicit Euler method is easy to implement and computationally inexpensive. However, it comes with significant drawbacks in terms of simulation accuracy. The biggest concern is that energy is not conserved as it should be, and unintuitively, the total energy increases over time. While the explicit Euler method can loosely simulate a simple pendulum, it is not recommended if accuracy is important.

A step up from the explicit Euler method is the semi-implicit Euler method, which provides a more accurate model while remaining as computationally efficient. This method conserves total energy, an important characteristic of the simple pendulum, though the energy fluctuates on a loose bound. However, there is still much room for improvement in tightening the bound on energy conservation.

The leapfrog method strikes a healthy balance between computational efficiency and model accuracy. As a symplectic integrator, it preserves the properties of the system, particularly energy conservation. Additionally, the leapfrog method is a second-order integrator, meaning it improves accuracy by tightening the bound on total energy fluctuations even further.

The GLRK4 method boasts the most impressive model accuracy at a relatively small computational cost. As a fourth-order symplectic integrator, it has an extremely tight bound on total energy fluctuations, making the deviation from the true solution practically nonexistent.

5.2 Double Pendulum Results

The results of our simulations clearly indicate that the Guass-Legendre Runge-Kutta integration method outperforms all of the other symplectic integrators we have implemented and tested. Lower-order methods such as Semi-Implicit Euler and Leapfrog failed to effectively conserve energy over time. Moreover, these methods perform computation using non-adaptive time-steps. Thus, error accumulates over time leading to the dissipation of energy. The chaotic behaviour of the double pendulum likely causes this accumulation, since no external forces are present in the system during our simulations which could explain this result.

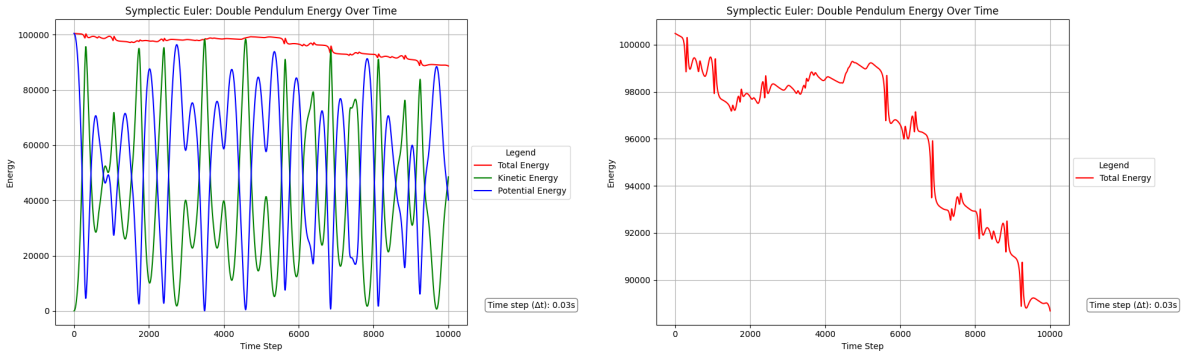

Figure 12: Symplectic Euler, Energy Over Time

The GLRK4 integration method shows the most promising results, as shown in Fig. 5. We can observe that the oscillation of total energy is tightly bound, and there is no notable dissipation of energy over time. However, the lower-order symplectic integrators may have some use when the initial angles of displacement θ_1 and θ_2 are small enough (i.e. each pendulum

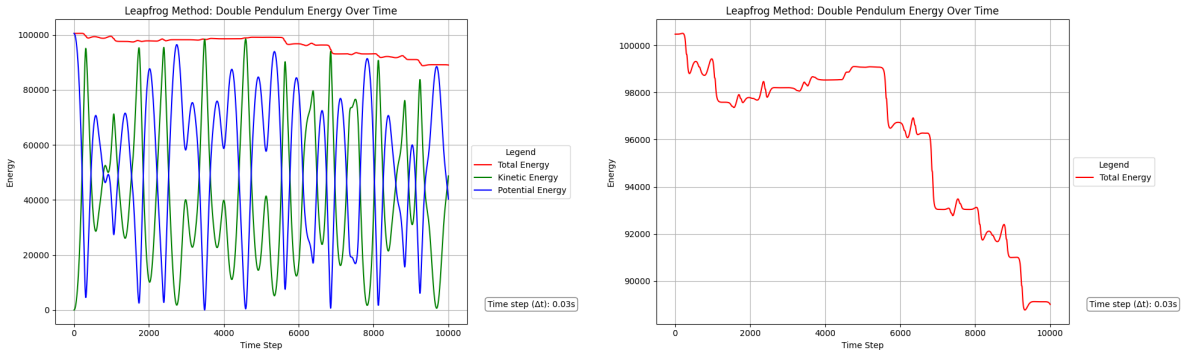

Figure 13: Leapfrog, Energy Over Time

exhibits simple oscillatory behaviour). Moreover, for such cases, the resource expenditure of applying the GLRK4 method may be computationally excessive.

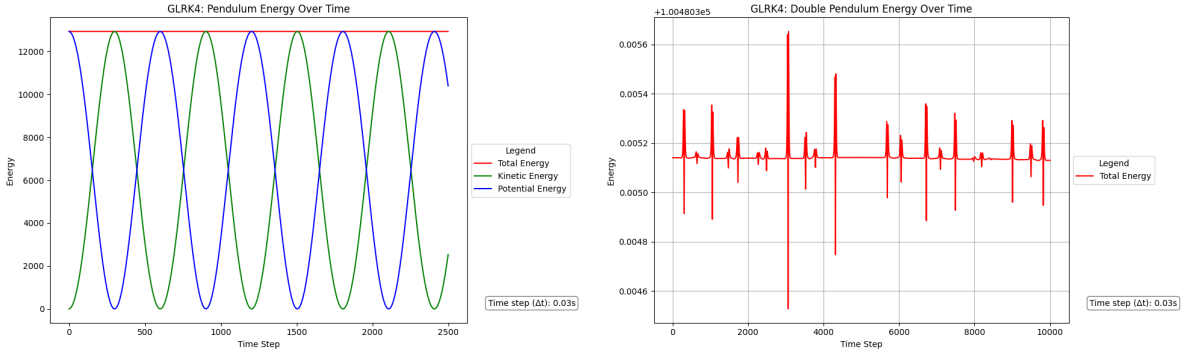

Figure 14: Guass-Legendre Runge-Kutta, Energy Over Time

6 Conclusions

Key Findings and Future Directions

Effectiveness of Symplectic Methods: Through our simulations, we found that symplectic methods are crucial for preserving the long-term energy behavior and true dynamics of chaotic systems like the double pendulum. Among the methods tested, the Gauss-Legendre RK4 (GLRK4) consistently outperformed others, providing superior accuracy and stability, particularly in more extended simulations.

Insights from Simulations: The most important aspect during simulations was the ability to maintain energy and accuracy in the system. Using a minimal step size proved to be sufficient for most tasks. However, non-symplectic methods exhibited significant artificial energy drift, especially during Double Pendulum simulations, whereas symplectic methods like GL-RK4 preserved the true behavior.

Future Work: Building on these results, some future studies that we could explore would be even more complex and chaotic systems. For example, the n-pendulum or higher-dimensional Hamiltonian systems. We believe that the lessons learned from taking on this ambitious project will help guide the development of robust numerical tools for our future investigations. Possibly

extending the analysis to coupled systems or quantum analogs could yield further insights into the interplay between chaos and the conservation of energy.

7 Bibliography

References

Baker, G. L. and J. A. Blackburn (2005). *The Pendulum*. Oxford Academic. DOI: 10.1093/oso/9780198567547.001.0001. URL: https://doi.org/10.1093/oso/9780198567547.001.0001.

Betzler, Nilis et al. (2008). "From the double pendulum model to full-body simulation: Evolution of golf swing modeling". In: *Sports Technology*.

Calvão, A M and T J P Penna (2015). "The double pendulum: a numerical study". In: *European Journal of Physics*.

Graichen, Knut, Michael Treuer, and Michael Zeitz (2007). "Swing-up of the double pendulum on a cart by feedforward and feedback control with experimental validation". In: *Automatica*.

Guo, By. and Zq. Wang (2009). "Legendre–Gauss collocation methods for ordinary differential equations". In: *Advances in Computational Mathematics* 30. Issue Date: April 2009, pp. 249–280. DOI: 10.1007/s10444-008-9067-6. URL: https://doi-org.myaccess.library.utoronto.ca/10.1007/s10444-008-9067-6.

Hairer, Ernst, Gerhard Wanner, and Christian Lubich (2006). *Geometric Numerical Integration: Structure-Preserving Algorithms for Ordinary Differential Equations*. Berlin, Heidelberg: Springer Berlin Heidelberg. DOI: 10.1007/3-540-30666-8.

Hernandez, David M. and Edmund Bertschinger (2015). "Symplectic integration for the collisional gravitational N-body problem". In: *Monthly Notices of the Royal Astronomical Society* 452.2, pp. 1934–1944. DOI: 10.1093/mnras/stv1439. URL: https://doi.org/10.1093/mnras/stv1439.

Meyer, Kenneth R. and Daniel C. Offin (2017). *Introduction to Hamiltonian Dynamical Systems and the N-Body Problem*. Third edition. Vol. 90. Cham: Springer Nature. DOI: 10.1007/978-3-319-53691-0.

Pettersen, Bjørn Rune (2016). "A historical review of gravimetric observations in Norway". In: *History of Geo- and Space Sciences* 7.2, pp. 79–89. DOI: 10.5194/hgss-7-79-2016. URL: https://doi.org/10.5194/hgss-7-79-2016.

Razafindralandy, Dina et al. (2019). "Some robust integrators for large time dynamics". In: *Advanced Modeling and Simulation in Engineering Sciences*.

Shanak, Hussein et al. (2021). "Some Features of Double Pendulum System - Numerical and Simulation Study". In: *Journal of Theoretical and Applied Mathematics*.

Tirapicos, Luís (2024). "Directions of precision: George Graham's instructions for his pendulum astronomical clocks". In: *Annals of Science* 81.1-2, pp. 124–138. DOI: 10.1080/00033790.2023.2282782. URL: https://doi.org/10.1080/00033790.2023.2282782.

Wang, Qun (2024). *MAT332 Introduction to Nonlinear Dynamics and Chaos*. 2nd.